International Journal of Heat and Mass Transfer 107 (2017) 846–861

Contents lists available at ScienceDirect

International Journal of Heat and Mass Transfer

journal homepage: www.elsevier.com/locate/ijhmt

Velocity and temperature profiles, wall shear stress and heat transfer coefficient of turbulent impinging jets

J.B.R. Loureiro *, A.P. Silva Freire

Mechanical Engineering Program (PEM/COPPE/UFRJ), C.P. 68503, 21941-972 Rio de Janeiro, Brazil

ARTICLE INFO

Article history:
Received 27 June 2016
Received in revised form 17 October 2016
Accepted 29 October 2016
Available online 19 November 2016

Keywords:
Impinging jet
Wall shear stress
Nusselt number
Parametric analysis

ABSTRACT

The purpose of this work is to present a set of empirical equations that can be used to predict the flow dynamics and the heat transfer properties of impinging jets over a wide range of Reynolds number, nozzle-to-plate spacing and radial position along the impingement plate. The parametrization scheme proposed by Loureiro and Silva Freire (Int. J. Heat Mass Transfer, 55 (2012), 6400–6409) is used here for the prediction of the mean flow field properties. In particular, the scaling for maximum velocity distribution along the impingement plate is extended to account for nozzle-to-plate distance and Reynolds number dependence. A new methodology for the calculation of the wall shear stress is also presented. The experimental data set of Guerra et al. (Int. J. Heat Mass Transfer, 48 (2005), 2829–2840) is used to propose a description of the full mean temperature profile for the wall jet region that follows a Weibull distribution. In all, eleven different experimental data sets are considered to propose working expressions that include a piecewise Nusselt number expression that furnishes a solution valid over the whole domain of the impingement plate, including the stagnation point and the wall jet region. New values are proposed for the power indexes and multiplicative parameters. The parametric analysis considers that the flow properties can be determined in terms of gross parameters like the free-jet momentum flux.

1. Introduction

Progress on the understanding of the fundamental physics of impinging jets is often troubled by the large number of parameters that are needed to define the problem. Very often authors limit their observations and theoretical analysis to the discussion of one or two aspects of specific interest. The inlet conditions (geometry and flow conditions), the nozzle-to-plate spacing, the effects of Reynolds number, the role of vortical structures, e.g., are a few of the many subjects of permanent interest.

The fragmented manner in which results are presented in literature naturally poses expected difficulties for the advancement of consolidated theories. For example, it is difficult to find a work where both the flow dynamics and the transfer of heat are discussed simultaneously. In particular, the experimental characterization of some parameters is notoriously difficult to find. The distributions of wall shear stress and local temperature profiles are typical examples.

The present work discusses both the velocity and temperature fields from the point of view of the theories introduced in Guerra et al. [1] and Loureiro and Silva Freire [2]. The parametrization scheme proposed by Loureiro and Silva Freire [2] for the maximum velocity distribution along the impingement plate is extended to account for nozzle-to-plate distance and Reynolds number dependence. The experimental results of Loureiro and Silva Freire [2] are used to validate a new methodology for the calculation of the wall shear stress. The turbulent impinging jet data set of Guerra et al. [1] is considered, to propose a description of the full mean temperature profile for the wall jet region that follows a Weibull distribution. The work also examines other nine different experimental data sets and ten different Nusselt number correlations to propose piecewise Nusselt number expressions, whose combination furnishes a solution that is valid over the whole domain of the impingement plate, including the stagnation point and the wall jet region. New values are proposed for the power indexes and multiplicative constants after a detailed analysis of eight different data sets is carried out.

The current new expressions are based on the data sets of Guerra et al. [1], Loureiro and Silva Freire [2], Poreh et al. [3], Fairweather and Hargrave [4], Fitzgerald and Garimella [5], Koseoglu and Baskayab [6], Huang and El-Genk [7], O'Donovan and Murray [8], Ozmen and Baydar [9], Katti and Prabhu [10] and Goldstein and Behbahani [11].

* Corresponding author.
E-mail address: jbrloureiro@gmail.com (J.B.R. Loureiro).

http://dx.doi.org/10.1016/j.ijheatmasstransfer.2016.10.105
0017-9310/

Nomenclature

A, A_1, A_2	parameters in velocity law of the wall
a, b, c	parameters in Nusselt number expressions
B, B_1, B_2	parameters in temperature law of the wall
C_1, C_2	parameters in power-law expressions
c_p	specific heat
D	nozzle diameter
h	heat transfer coefficient
H	nozzle-to-plate distance
k	thermal conductivity
n_1 to n_5	parameters in the correlations for Nusselt number
m_1, m_2	parameters in power-law expressions
M_j	jet momentum flux ($=DU_j^2$)
N_u	Nusselt number ($=hD/k$)
P_r	Prandtl number ($=\nu/\alpha$)
q_w	wall heat flux
r	radial distance on the impingement plate
R_e	Reynolds number ($=(DM_j)^{1/2}/\nu$)
T_j	free-jet temperature
T_w	wall temperature
t_τ	friction temperature ($=q_w/(\rho c_p u_\tau)$)
U, u	longitudinal velocity component
U_j	jet bulk velocity
u_τ	friction velocity
r, y	flow cartesian coordinates located at the center of the impingement plate
$y_{0.5}$	position of the half-maximum value (for velocity and temperature distributions).

Greek symbols

α	thermal diffusivity ($=k/(\rho c_p)$)
$\beta, \gamma, \lambda, \sigma, \zeta$	parameters in Weibull distribution
Δ_1	shape factor for the velocity distribution in the wall jet region
$\varkappa$	von Karman's constant (=0.4)
$\varkappa_t$	von Karman's constant, temperature profile (=0.44)
μ	absolut viscosity
μ	mean value
ν	kinematic viscosity
ρ	density
σ	standard deviation
τ	shear stress.

Subscripts

min	local minimum
max	local maximum
w	wall condition

The use of analytical or empirical expressions for the description of complex problems offers obvious advantages in desired applications. The non-linear and multi-scale character of the Navier–Stokes equations for high-Reynolds number flows makes any attempt at resolving the smallest dynamically important scales an extremely difficult affair due to the very fine meshes and time steps that must be considered. Even numerical approaches that resort to averaged equations and closure modelling are very expensive. The objective implication is that methods which resort to local perturbation techniques, parametric analysis and experimental correlations can be very useful to introduce near wall solutions. These methods define simple working rules and predictive mathematical relations to describe the main characteristics of rapidly varying local solutions [12,13].

Many authors emphasize that one issue that needs to be adequately discussed is the high heat and mass transfer characteristics of impinging jets. The existing voluminous bibliography on the experimental, theoretical and numerical aspects of the problem has not, for instance, completely explained the appearance of distinct peaks in the radial distribution of the Nusselt number [14]. The adequacy of turbulence models and near-wall approaches is also a subject of considerable dispute as argued by Pulat et al. [15].

The analysis conducted in the present work follows the approach introduced by Narasimha et al. [13] and considers that the flow properties can be determined in terms of gross parameters like the jet momentum flux ($=DU_j^2$) and the wall heat flux (q_w). The existence of near wall logarithmic regions for the velocity and temperature fields is also considered as presumed by Özdemir and Whitelaw [16], Guerra et al. [1] and Loureiro and Silva Freire [2].

2. Impinging jet flow configuration

The complex configuration of the flow dynamics of an impinging jet has been illustrated in the visualization study of Popiel and Trass [17]. The existence of large-scale ordered structures is evident and determines much of the flow properties as discussed in the LES simulation results of Uddin et al. [14]. The evolution and breakdown of the jet ring vortices is further discussed in the LES investigation of Hadziabdi and Hanjalic [18].

A theoretical treatment of impinging jets is possible provided the flow domain is divided into regions where dominant physical effects can be singled out and local solutions found. One common procedure is to divide the flow into four regions. The four regions identified by Poreh et al. [3] are: the free-jet transition region, the free-jet region, the deflection zone and the radial wall jet (see Fig. 1). The classification of Phares et al. [19] divides the flow into the free jet region (consisting of near-field and far-field regions), the inviscid impingement region, the impingement boundary layer and the wall jet region (see Fig. 2). Of course, both pictures of the flow can be merged provided the deflection zone of Poreh et al. [3] is seen as a combination of the inviscid impingement region and the impingement boundary layer.

In their analytical approach to problem solution, Phares et al. [19] propose inviscid and boundary layer solutions to determine the wall shear stress in the small region of flow located just above

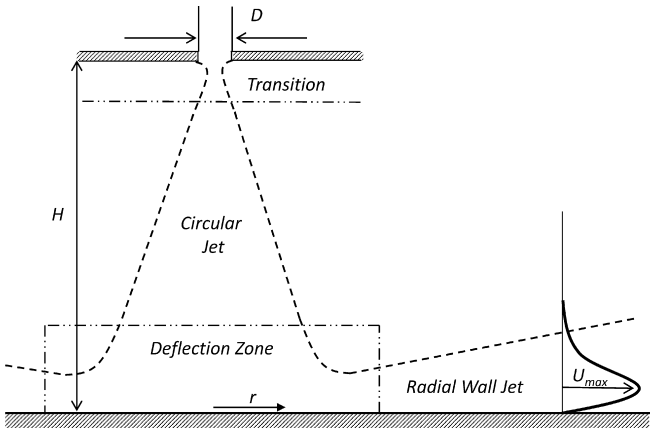

Fig. 1. Impinging jet flow configuration according to Poreh et al. [3].

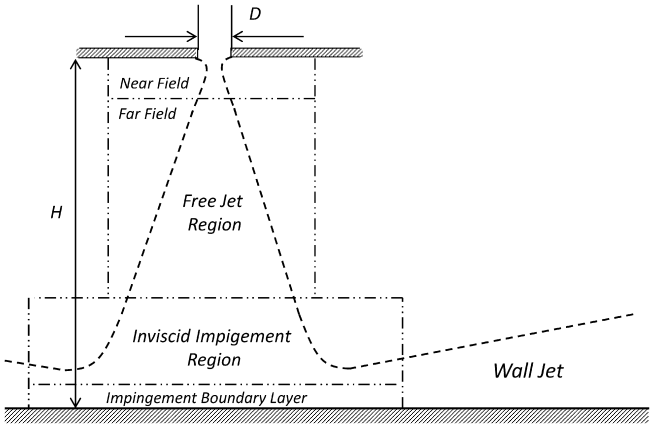

Fig. 2. Impinging jet flow configuration according to Phares et al. [19].

the impingement plane. Poreh et al. [3] concentrate their analysis in the region of radial wall jet. The present developments deal mostly with the wall jet region, but not exclusively. Poreh et al. [3] applied an integral method to the boundary layer equation and similarity arguments to arrive at a power-law relation between the radial position and the magnitude of the maximum wall jet velocity. Here, a similar hypothesis is used.

3. Flow dynamics in the wall jet region

Regarding the velocity field, Phares et al. [19] develop integral analytical solutions for the inviscid impingement region and the impingement boundary layer. In the wall jet region, however, predictions of the wall shear stress are provided by the empirical expression of Poreh et al. [3].

The wall jet region of an impinging jet is studied by Loureiro and Silva Freire [2] through the parametric approach suggested by Narasimha et al. [13]. The latter authors propose that at sufficiently large distances downstream of the issuing nozzle the flow dynamics is governed by the total momentum flux at the jet exit (M_j) and viscosity. In Loureiro and Silva Freire [2] near wall laser-Doppler anemometry data are used to determine the friction velocity through the linear portion of the velocity profile, so that the logarithmic behavior of the near wall velocity distribution can be studied unambiguously.

Özdemir and Whitelaw [16] suggest that a Weibull distribution (Eq. (1)) can be used to represent the global features of the mean velocity profile as:

$$\frac{U}{U_{max}} = \frac{\gamma}{\beta}\left(\frac{y/y_{0.5}}{\beta}\right)^{\gamma-1}\exp\left(-\left(\frac{y/y_{0.5}}{\beta}\right)^{\gamma}\right), \tag{1}$$

where the constant values $\gamma = 1.32$ and $\beta = 0.73$ calculated by Loureiro and Silva Freire [2] corroborate previous results of Özdemir and Whitelaw [16]. At a certain distance from the wall where the maximum velocity takes place, the above equation furnishes the relation $y_{0.5} = y_{max}/0.2495$.

Özdemir and Whitelaw [16] have also shown that near the wall a logarithmic velocity profile is observed with a level, A, that obeys a scaling law based on the stream-wise evolution of the flow characterized by its maximum velocity, U_{max}. Thus, according to Özdemir and Whitelaw [16] the nozzle diameter is an inappropriate reference scaling.

To describe the logarithmic velocity profile, Özdemir and Whitelaw [16] propose an expression of the form:

$$\frac{U}{u_\tau} = \frac{1}{\varkappa}\ln\left(\frac{yu_\tau}{\nu}\right) + A, \tag{2}$$

with

$$A = A_1\frac{U_{max}}{u_\tau} - A_2, \tag{3}$$

where $\varkappa = 0.4$, u_τ denotes the friction velocity and A_1 and A_2 must be experimentally determined. The experimental data of Loureiro and Silva Freire [2] implies that $A_1 = 0.962$ and $A_2 = 9$.

The analysis of Loureiro and Silva Freire [2] was carried out for one nozzle-to-plate distance ($H/D = 2$) and Reynolds number (= 47,100). To extend those results to further experimental conditions, consider the simple mass balance across the control volume indicated in Fig. 3.

The impinging jet flows with a bulk velocity U_j through a nozzle of diameter D and spreads radially over the impact plate located at a distance H from the nozzle. The mass conservation equation yields

$$\frac{\pi D^2}{4}U_j = \Delta_1(2\pi rH)U_{max}, \tag{4}$$

where Δ_1 (<1) denotes a shape factor related to the structure of the velocity distribution at the wall jet region (section B'B of Fig. 3). The shape factor Δ_1 expresses the relation between the mean velocity U_{mean} and U_{max}, so that U_{max} can be explicited from Eq. (4) as:

$$U_{max} = \frac{1}{8\Delta_1}\frac{D}{H}\frac{D}{r}U_j. \tag{5}$$

As suggested by Narasimha et al. [13], we consider that the flow dynamics is governed by the jet momentum flux M_j, so that the above equation can be re-written as:

$$\frac{U_{max}\nu}{M_j} = C_1R_e\frac{D}{H}\left(\frac{rM_j}{\nu^2}\right)^{m_1}, \quad M_j = DU_j^2, \tag{6}$$

where the shape factor has been generalized as a constant C_1. The theoretical development suggests $m_1 = -1$. This value, however, needs to be validated through experimental data.

The position where U_{max} occurs can be predicted through the relation introduced by Loureiro and Silva Freire [2]:

$$\frac{y_{max}M_j}{\nu^2} = C_2\left(\frac{rM_j}{\nu^2}\right)^{m_2}. \tag{7}$$

The constants C_1, m_1, C_2 and m_2 must be experimentally determined.

Given y_{max}, evaluated through Eq. (7), the quantity $y_{0.5}$ can be determined from Eq. (1).

The above equations can be used to develop a simple method to determine the friction velocity from the logarithmic law of the wall. First, solve Eq. (1) at any location inside the logarithmic region, say, the point $y_c = 0.6y_{max}$ to yield U_c. The pair (y_c, U_c) can then be substituted into Eq. (2) to find u_τ.

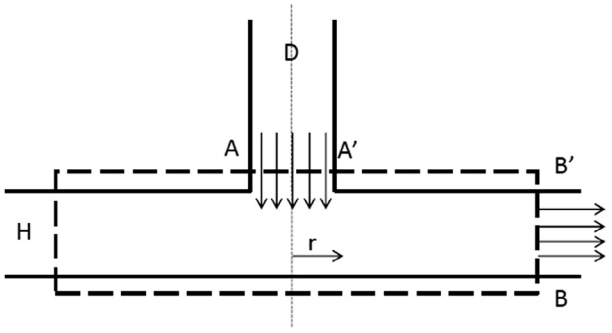

Fig. 3. Control volume for the impinging jet.

4. Heat transfer behavior of impinging jets

The prediction of the heat transfer behavior of impinging jets is based on non-dimensional equations written in terms of Nusselt, Prandtl and Reynolds numbers. The functional form of those equations is typically derived from analytical solutions for an axisymmetric jet impinging normally onto a flat surface, where a laminar boundary layer develops.

In contrast to the flow field configuration discussed above, the regions of validity of the heat transfer correlations are not clearly defined. In the work of Liu et al. [20], the integral solutions for impinging liquid jets are derived for a domain divided into five different regions: (i) stagnation zone, (ii) transition region, (iii) laminar boundary layer, (iv) similarity region and (v) turbulent region. These authors argue that the configuration of the heat transfer regions are more complicated than those for the flow field since more parameters are involved. For the domain definition, Liu et al. [20] base their arguments on the relative importance between the momentum and the thermal boundary layer thicknesses.

In analogy to the flow configuration used by Poreh et al. [3], Katti and Prabhu [10] divide the thermal field into three regions: (i) a stagnation region, valid over the interval $0 < r/D < 1$, (ii) a transition region, in the range $1 < r/D < 2.5$, and (iii) a wall jet region that extends over $r/D > 2.5$. In the present work, we follow the configuration suggested by Katti and Prabhu [10], as illustrated in Fig. 4.

The description of Nusselt number in literature considers cases with varying nozzle geometry, nozzle-to-plate distance, jet inclination, confinement, roughness, wall curvature, Reynolds number, Prandtl number and turbulent intensity, among other factors. Normally, most of the available correlations describe the average heat transfer coefficient. Correlations can be found for the stagnation point and the local Nusselt distribution along an impingement plate. However, the development of equations for prediction of the peak values in the distribution of Nusselt number is a matter that still deserves consideration.

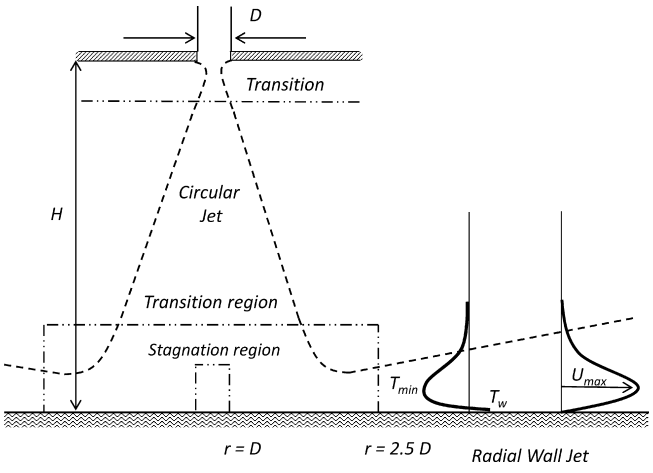

Fig. 4. Impinging jet heat transfer configuration according to Katti and Prabhu [10].

The present work studies the performance of ten different correlations for the stagnation Nusselt number and ten correlations for the Nusselt number radial distribution. These equations are valid for constant heat flux at the wall and were selected for discussion after a thorough literature review. The purpose here is to identify the range of application of the equations to variations in Reynolds number, nozzle-to-plate spacing and downstream distance from the impingement point.

In general, the correlations presented in literature have been proposed and validated against a limited set of experiments. This poses serious restrictions to their predictive capability, for the embedded constants have been calibrated against just a specific configuration. We anticipate that none of the correlations investigated in this work furnishes accurate predictions for the whole investigated domain.

4.1. Nusselt number correlations: stagnation point

Table 1 shows the stagnation Nusselt number correlations investigated in the present work. Table 1 also presents the range of Reynolds number, nozzle-to-plate distance and nozzle diameter for which each correlation was derived.

The correlation of Katti and Prabhu [10] is based on the work of Brdlik and Savin [28]. The latter work considers a constant value for a_1 (see Table 1); Katti and Prabhu [10] on the other hand have suggested this parameter to vary with H/D.

For a laminar incompressible jet impinging on a flat surface, the Navier–Stokes equations can be simplified to an analytical solution of the form $N_{u_0} = CR_e^{1/2}Pr^{2/5}$ [21,24,29–31]. Table 1 shows that the correlations proposed by Liu et al. [20], Donaldson [21], Liu and Sullivan [24] and Zumbrunnen and Aziz [26], all follow this approach, implying that any dependence on H/D is not accounted for.

4.2. Nusselt number correlations: radial distribution

Viskanta [30] comments that turbulent heat transfer rates can reach values 1.4 to 2.2 times higher than those resulting from the laminar problem. The entrainment of the surrounding fluid and the decay of the centerline jet velocity make the nozzle-to-plate distance play a major role on the transfer of heat, specially as H/D increases. Viskanta also comments that the large number

Table 1
Correlations for the stagnation point Nusselt number N_{u_0}.

Reference	R_e	D [mm]	H/D	Correlation
Ozmen and Baydar [9]	30,000–70,000	12.60	1–10	$N_{u_0} = 0.092R_e^{0.69}(H/D)^{0.019}$
Katti and Prabhu [10]	12,000–28,000	7.35	0.5–8	$N_{u_0} = a_1R_e^{0.5}P_r^{1/3}(H/D)^{-0.11}$
Liu et al. [20]	2,000–4,000	3.8, 9.5		$N_{u_0} = 0.715R_e^{0.5}P_r^{1/3}$
Donaldson [21]				$N_{u_0} = 0.752P_r^{0.5}R_e^{0.5}$
Lytle and Webb [22]	3,600–27,600	7.8–10.9	0.1–6	$N_{u_0} = 0.726R_e^{0.53}(H/D)^{-0.191}$
San and Shiao [23]	10,000–30,000	1.5, 3, 6, 9	1–6	$N_{u_0} = 0.426R_e^{0.638}(H/D)^{-0.3}$
Liu and Sullivan [24]	12,000–15,100	12.7	1–2	$N_{u_0} = 0.585R_e^{0.5}P_r^{0.4}$
Garimella and Rice [25]	4,000–23,000		1–5	$N_{u_0} = 0.462R_e^{0.585}P_r^{0.4}(H/D)^{0.024}$
Zumbrunnen and Aziz [26]	3,100–20,750		7	$N_{u_0} = 0.230R_e^{0.589}P_r^{0.4}$
Mohanty and Tawfek [27]	4,860–15,300	5, 7	9–39.6	$N_{u_0} = 0.388R_e^{0.696}(H/D)^{-0.345}$

Table 2
Correlations for Nusselt number prediction in the radial direction.

Reference	R_e	H/D	r/D	Correlation
Gardon and Cobonpue [32]	> 2,000	> 12	0–12	$N_u = 1.811R_e^{0.55}P_r^{0.33}(H/D)^{-0.55}(r/D)^{-0.45}$
Huang and El-Genk [7]	6,000–60,000	1–12	0–10	$N_u = R_e^{0.76}P_r^{0.42}(a + b(H/D) + c(H/D)^2)$
Goldstein et al. [33]	61,000–124,000	> 6	0.5–32	$N_u = R_e^{0.76}\frac{24-\lvert H/D-7.75\rvert}{533+44(r/D)^{1.394}}$
Jambunathan et al. [34]	5,000–124,000	1.2–16	< 6	$N_u = KR_e^a(1-(r/D)^n)^{-1}$
Martin [35]	> 2,000			$N_u = 1.36R_e^{0.574}P_r^{0.42}(D/r)\frac{1-1.1(D/r)}{1+0.1(H/D-6)(D/r)}$
Liu et al. [20]	2,000–4,000		0–20	$N_u = (8R_eP_rS_t)(49(H/r)(r/D) + 28(r/D)^2St) - 1$
Katti and Prabhu [10]	12,000–28,000	0.5–8	0–1	$N_u = aR_e^{0.5}P_r^{1/3}(H/D)^{-0.11}(1-b^{-1}(r/D)^2(H/D)^{-0.2})^{1.2}$
Katti and Prabhu [10]	12,000–28,000	$\leqslant 3.0$	1–2.5	$N_u = 0.2636R_e^{0.6188}(H/D)^{-0.0898}(r/D)^{-0.074}$
Katti and Prabhu [10]	12,000–28,000	$\geqslant 4.0$	1–2.5	$N_u = 0.1980R_e^{0.6632}(H/D)^{-0.0826}(r/D)^{-0.3702}$
Katti and Prabhu [10]	12,000–28,000	0.5–8.0	$\geqslant 2.5$	$N_u = 0.0436(E)R_e^{0.8}P_r^{0.33}(H/D)^{0.0976}(r/D)^{-1.0976}$

of parameters involved in the heat transfer problem naturally gives origin to many different correlations in literature.

The correlations investigated in the present work are listed in Table 2, together with the ranges of validity as specified in the original references.

Liu et al. [20] recognize that the turbulent Nusselt number is substantially higher than that for the transfer of heat in laminar flows. To account for the turbulent effects, the authors derive a Nusselt equation from the thermal law of the wall, with Stanton number defined as $S_t = q_w/(\rho c_p U_{max}(T_w - T_j))$.

The work of Jambunathan et al. [34] presents an extensive review of experimental results for single impinging jet flow configurations. Based on the collected data, the authors propose the equation shown in Table 2, where K is a constant that varies for $r/D < 2$ and n is a parameter that varies between 1 and 2. The Reynolds number dependence is accounted for by a power law exponent that depends on the nozzle-to-plate spacing and the radial distance from the stagnation point.

All the correlations listed in Tables 1 and 2 are tested against the reference experimental data discussed in the next section. Once the parametric equations are defined, a non-linear fitting procedure of the original functional form to the complete set of experimental data is carried out to determine an appropriate set of constants. This procedure, of course, furnishes a new set of equations that is now valid for broader domains of Reynolds number, nozzle-to-plate distance and downstream radial distance.

4.3. Temperature profile over the impingement plate

The inner temperature profile is shown by Guerra et al. [1] to follow a logarithmic solution, that is,

$$\frac{T_w - T}{t_\tau} = \frac{1}{\varkappa_t}\ln\left(\frac{yu_\tau}{\nu}\right) + B, \tag{8}$$

with

$$B = B_1\left(\frac{T_w - T_{min}}{t_\tau}\right) - B_2, \tag{9}$$

where $B_1 = 1.003$ and $B_2 = 9.462$.

In the above equation, t_τ is the friction temperature ($=q_w/(\rho c_p u_\tau)$), u_τ is the friction velocity ($=\sqrt{\tau_w/\rho}$) and $\varkappa_t = 0.44$.

Most data in literature are presented in terms of parameters encapsulated in non-dimensional groups. The heat transfer of impinging jets is normally reported in terms of the Nusselt number. While in most situations this practice allows comparisons between experiments to be a straightforward affair, sometimes it may also make difficult the recovery of primitive parameters, such as the wall heat flux and the friction velocity, for the validation of theories. Most works do not report the statistics of the velocity and temperature fields. For example, local temperature profiles were only found in one reference, Guerra et al. [1].

The results on the temperature field reported in the work of Guerra et al. [1] suggest that the temperature profile follows a modified Weibull distribution, according to:

$$\frac{T_w - T}{T_w - T_{min}} = \frac{\sigma}{\lambda}\left(\frac{y/y_{0.5}}{\lambda}\right)^{\sigma-1}\exp\left(-\left(\frac{y/y_{0.5}}{\lambda}\right)^{\sigma}\right) + \exp\left(-\left(\frac{y/y_{0.5}}{\lambda}\right)^{\zeta}\right), \tag{10}$$

where T_w = wall temperature, T_{min} = minimum temperature in the temperature profile, y_{min} = height of minimum temperature, σ, λ and ζ must be determined from experimental results, and the last exponential term has been added since as $y \to \infty$, $T \to T_j$.

The position of y_{min} is here considered to coincide with the position of y_{max} (Eq. (7)), as shown in Fig. 4. Thus, with the use of Eqs. (8) and (10), T_{min} can then be determined.

5. Results

In the present section, the appropriate set of parametric equations that is to be used in the prediction of the flow dynamics and heat transfer of impinging jets is introduced. Results for the validation of the scaling laws introduced for the velocity field are shown first. The Nusselt number correlations are presented next.

Table 3
Flow conditions.

Work	R_e	D [mm]	H/D	Confinement	m_1
Guerra et al. [1]	35,000	43.5	2	Yes	−1.05
Loureiro and Silva Freire [2]	47,100	43.5	2	Yes	−0.99
Poreh et al. [3]	161,000	50.8	12	No	−1.09
Poreh et al. [3]	196,000	50.8	12	No	−1.1
Fairweather and Hargrave [4]	18,800	13.3	2	No	−0.94
Fitzgerald and Garimella [5]	23,000	3.18	4	Yes	−1.08
Koseoglu and Baskayab [6]	10,000	10	2	Yes	−1.05
Koseoglu and Baskayab [6]	10,000	10	6	Yes	−0.94

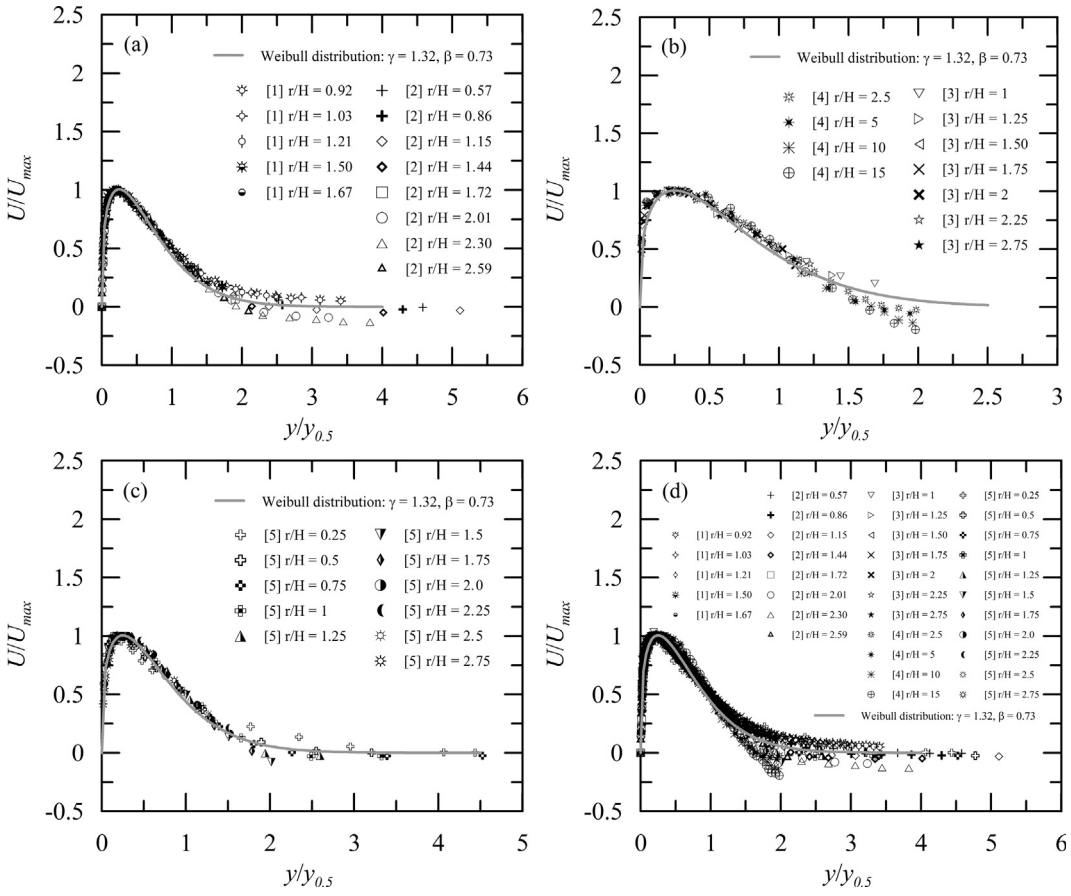

Fig. 5. Weibull distribution for the mean velocity profile with $\gamma = 1.32$, $\beta = 0.73$: (a) data of Guerra et al. [1] and Loureiro and Silva Freire [2], (b) Poreh et al. [3] and Fairweather and Hargrave [4], (c) Fitzgerald and Garimella [5], (d) all 35 velocity profiles.

The proposed Weibull distribution for the temperature field is validated against the data of Guerra et al. [1].

5.1. Scaling laws for the flow field

To characterize the parameters appearing in Eqs. (1)–(7), various sets of experimental results are considered [1–6]. The reference flow conditions are shown in Table 3. This data set includes both confined and unconfined jet flow configurations. The range of nozzle-to-plate spacing (H/D) varies from 2 to 12; the Reynolds number changes from 10,000 to 196,000. The jet orifice diameter varies from 3.18 mm to 50.8 mm.

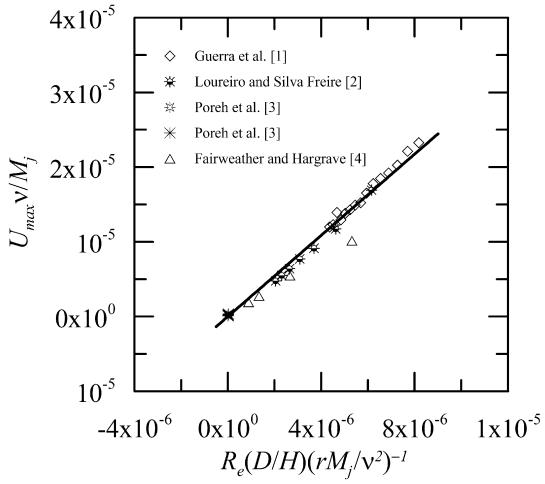

Fig. 6. Dependence of U_{max} with the radial distance.

The adequacy of a Weibull distribution, Eq. (1), to the description of the mean velocity profile in the wall region is demonstrated in Fig. 5a-d. In order to allow identification of the different velocity profiles, the data of Guerra et al. [1] and Loureiro and Silva Freire [2] are shown in Fig. 5a, while the results of Poreh et al. [3] and Fairweather and Hargrave [4] (Fig. 5b), and Fitzgerald and Garimella [5] (Fig. 5c) are shown separately.

Fig. 5d introduces 35 velocity profiles from five different experimental works [1–5], normalized according to the Weibull distribution suggested by Özdemir and Whitelaw [16]. Data shown here include confined and unconfined jets and cover a wide length over the impingement plate. The jet to plate spacing varies in the range of $2 < H/D < 12$, while the Reynolds number ranges from 10,000 to 196,000. A complete similarity of the velocity distribution is obtained through the scaling parameters U_{max} and $y_{0.5}$, the distance away from the wall where the velocity reaches half of its maximum value. The constants $\gamma = 1.32$ and $\beta = 0.73$ correspond to the values previously calculated by Loureiro and Silva Freire [2]. The results shown in Fig. 5d present a good agreement between Eq. (1) and the experimental data.

The behavior of the newly proposed correlation for U_{max}, given by Eq. (6), is shown in Fig. 6, where $m_1 = -1$ and $C_1 = 2.72$. To find m_1 and C_1, the data on maximum velocity were initially plotted in log–log coordinates, as suggested by the normalization indicated in Eq. (6). Next, a best fit was chosen for every profile by searching for the maximum coefficient of determination, R-squared. Other statistical parameters were also observed, the residual sum of squares and the residual mean square. Normally, a coefficient of determination superior to 0.99 was obtained.

The values of m_1 for each data set ranged from −0.94 to −1.1 (see Table 3) with the average value of $\mu_{m1} = -1.02$ and the standard deviation $\sigma_{m1} = 0.057$. Here, we have then fixed $m_1 = -1$, the value that resulted from the mass conservation equation (Fig. 3). Once m_1 had been determined, a best fit was further applied to all data simultaneously, resulting in the final value of $C_1 = 2.72$ with a R-squared value of 0.994.

The determination of the constants present in Eq. (7), which describes the location of the maximum velocity along the impingement plate, y_{max}, is shown in Fig. 7. In analogy to the procedure used to determine the constants m_1 and C_1 of Eq. (6), the exponent m_2 was firstly evaluated from independent curve fittings of y_{max} for each data set, plotted according to the variables indicated in Eq. (7). Estimated values of m_2 varied between 0.91 and 1.2, with a mean value of $\mu_{m2} = 0.985$ and a standard deviation $\sigma_{m2} = 0.091$. Once m_2 was fixed equal to unity, the value of C_2 was determined (= 0.0175) with a R-squared value of 0.994.

A methodology based on the law of the wall, Eqs. (2) and (3), for the prediction of the wall shear stress is presented next.

First, solve Eq. (1) at any location inside the logarithmic region, for example, at a given point located at $y_c = 0.6y_{max}$, to yield U_c. The pair (y_c, U_c) located inside the fully turbulent region of the wall jet can then be substituted into Eq. (2) to find u_τ.

Wall shear stress predictions based on the above procedure are shown in Fig. 8 in comparison to the experimental data of Loureiro and Silva Freire [2]. These data are particularly accurate for they result from a direct measurement of the velocity distribution in the viscous sublayer [36]. Fig. 8 includes for reference the empirical correlation suggested in the work of Poreh et al. [3].

The good agreement between the wall shear stress predictions (Eqs. (2) and (3)) and the experimental data is seen for the wall jet region, $r/D > 2.5$. Figs. 5–8 show unambiguously that the set of Eqs. (1)–(7) can be used to predict the characteristics of the flow field of impinging jets, such as the mean velocity, the position and intensity of the maximum velocity and the wall shear stress.

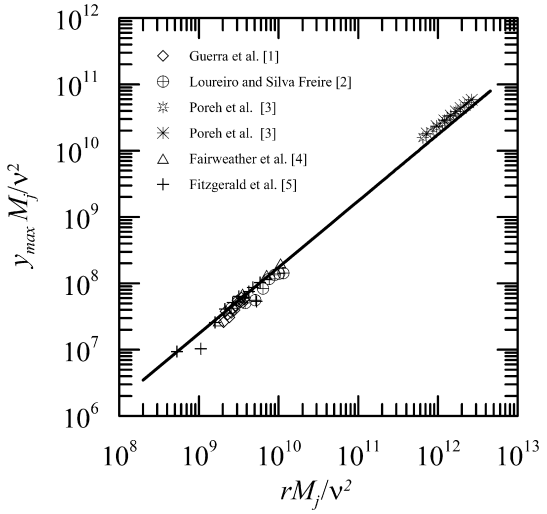

Fig. 7. Dependence of y_{max} with the radial distance.

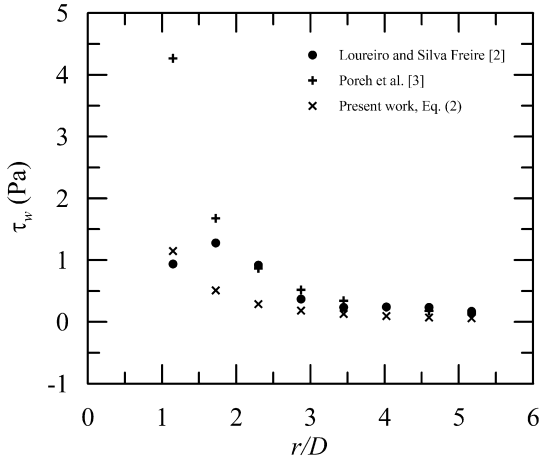

Fig. 8. Comparison of the wall shear stress prediction through Eqs. (2) and (3) with the experimental data of Loureiro and Silva Freire [2] and the correlation of Poreh et al. [3].

5.2. Parametric relations for the transfer of heat

To characterize the heat transfer behavior of impinging jets, the experimental results of references [1,7–11,37] are considered. The experimental conditions are shown in Table 4. Data for confined and unconfined flows, with nozzle-to-plate spacing in the range $0.5 < H/D < 10$, and Reynolds number varying from 6,000 to 70,000 are considered.

The typical behavior of Nusselt number according to the data of [8–10] is illustrated in Fig. 9. The double peak structure is clearly visible for H/D lower than about 4. Discussion on the physics of the second peak has occupied many authors. Hadziabdi and Hanjalic [18] argue that the reattachment of the recirculation bubble – and the associated turbulence production – is the main cause. However, the simulations of Uddin et al. [14] do not present a recirculation bubble, which leads authors to attribute the second peak to the higher turbulence in the boundary layer as a result of the strong flow acceleration and shear.

5.2.1. Nusselt number correlation: stagnation point

The correlations in Table 1 are here tested against a host of experimental data. This is shown next.

Fig. 10a and 10b show, respectively, the N_{u_0} data of Huang and El-Genk [7] and O'Donovan and Murray [8] as compared to the correlations of Zumbrunnen and Aziz [26], Ozmen and Baydar [9] and Liu et al. [20]. Fig. 10a shows a good agreement for the correlation of Ozmen and Baydar [9], for all the range of R_e and H/D; the correlation of Zumbrunnen and Aziz [26] only presents good prediction in the range of Reynolds number $R_e < 20,000$. Fig. 10b

Table 4
Heat transfer conditions.

Work	R_e	D [mm]	H/D	Confinement
Guerra et al. [1]	35,000	43.5	2	Yes
Huang and El-Genk [7]	6,000–60,000	6.2	1–10	No
O'Donovan and Murray [8]	10,000–30,000	13.50	0.5–8	No
Ozmen and Baydar [9]	30,000–70,000	12.6	1–10	No
Katti and Prabhu [10]	12,000–28,000	7.35	0.5–8	No
Goldstein and Behbahani [11]	35,100–121,000	12.7	6–12	Yes
Fenot et al. [37]	23,000	10.0	2, 5	Yes/No

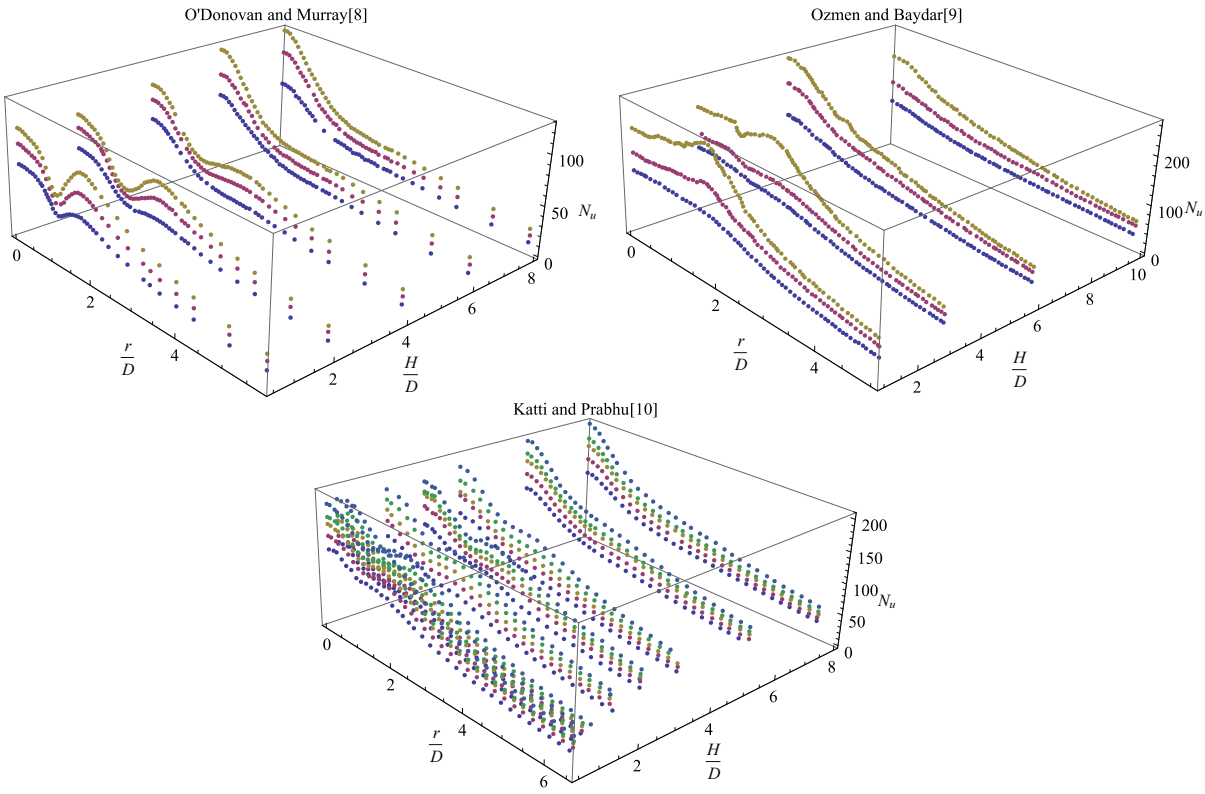

Fig. 9. Typical behavior of N_u according to references [8–10].

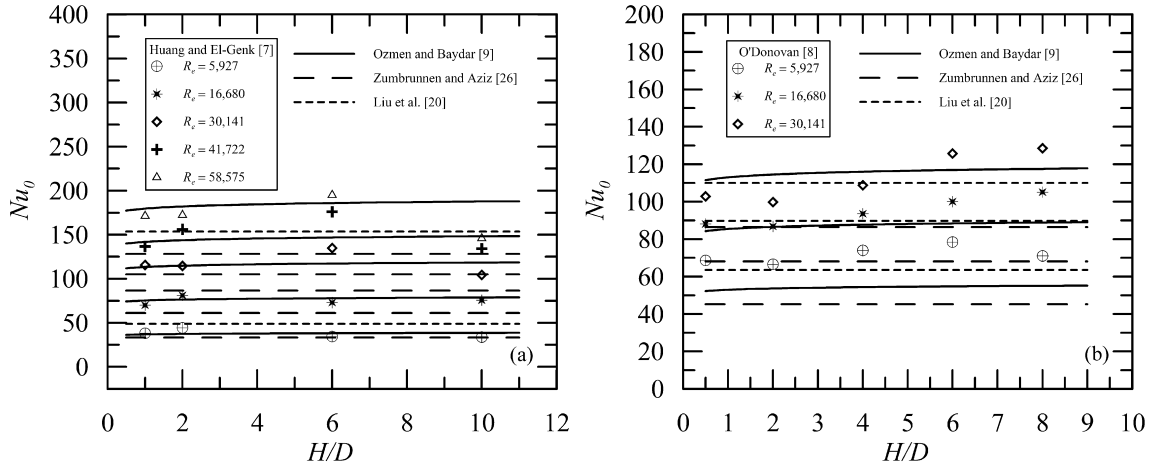

Fig. 10. Comparison of N_{u_0} correlations against the reference experimental data.

shows that the correlation of Ozmen and Baydar [9] underestimates predictions for the low values of R_e, but provides good predictions for the high values of R_e. The correlation of Zumbrunnen and Aziz [26] much underestimates Nusselt numbers for all considered Reynolds numbers. The correlation of Liu et al. [20] presents good agreement with the data shown in Fig. 10b.

Viskanta [30] comments that N_{u_0} typically shows peak values around H/D ranging from 6 to 8. As seen from Fig. 10a and 10b,

Table 5
Fitting statistics for the selected functional forms: prediction of the stagnation Nusselt number.

Formulation	Const. a	Const. b	Const. c	CI (a)	CI (b)	CI (c)	R-sq
$N_{u_0} = aR_e^{1/2}P_r^{1/3}$	0.868	–	–	(0.823, 0.914)	–	–	0.964
$N_{u_0} = aR_e^{b}P_r^{1/3}$	0.159	0.656	–	(0.027, 0.291)	(0.581, 0.732)	–	0.973
$N_{u_0} = aR_e^{b}(H/D)^{c}$	0.135	0.661	−0.009	(0.017, 0.254)	(0.579, 0.744)	(−0.065, 0.048)	0.973
$N_{u_0} = aR_e^{1/2}P_r^{1/3}(H/D)^{c}$	0.826	–	0.033	(0.739, 0.914)	–	(−0.027, 0.093)	0.964

even correlations that account for the H/D dependence do not correctly reflect this behavior.

The average percentage error between the estimated and measured values of N_{u_0} is as follows: (i) Ozmen and Baydar [9]: within 9% to 14%, (ii) Liu et al. [20]: within 9% to 18%, and (iii) Zumbrunnen and Aziz [26]: within 21% to 29%. The other correlations mentioned in Table 1 provide average percentage error of 30% or higher.

The correlations of references [9] and [20] present similar agreement, but their functional forms are based on different premises. Reference [9] takes into account the influence of H/D, whereas reference [20] considers the classical laminar theory

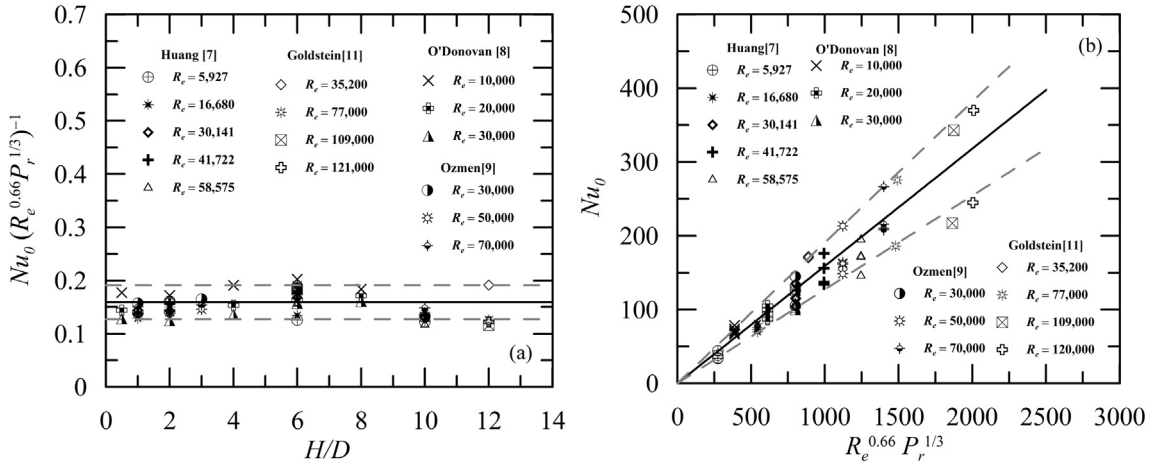

Fig. 11. Stagnation Nusselt number data of references [7–9,11] and correlation given by Eq. (11): (a) behaviour against H/D and (b) dependence with $R_e^{0.66}P_r^{1/3}$.

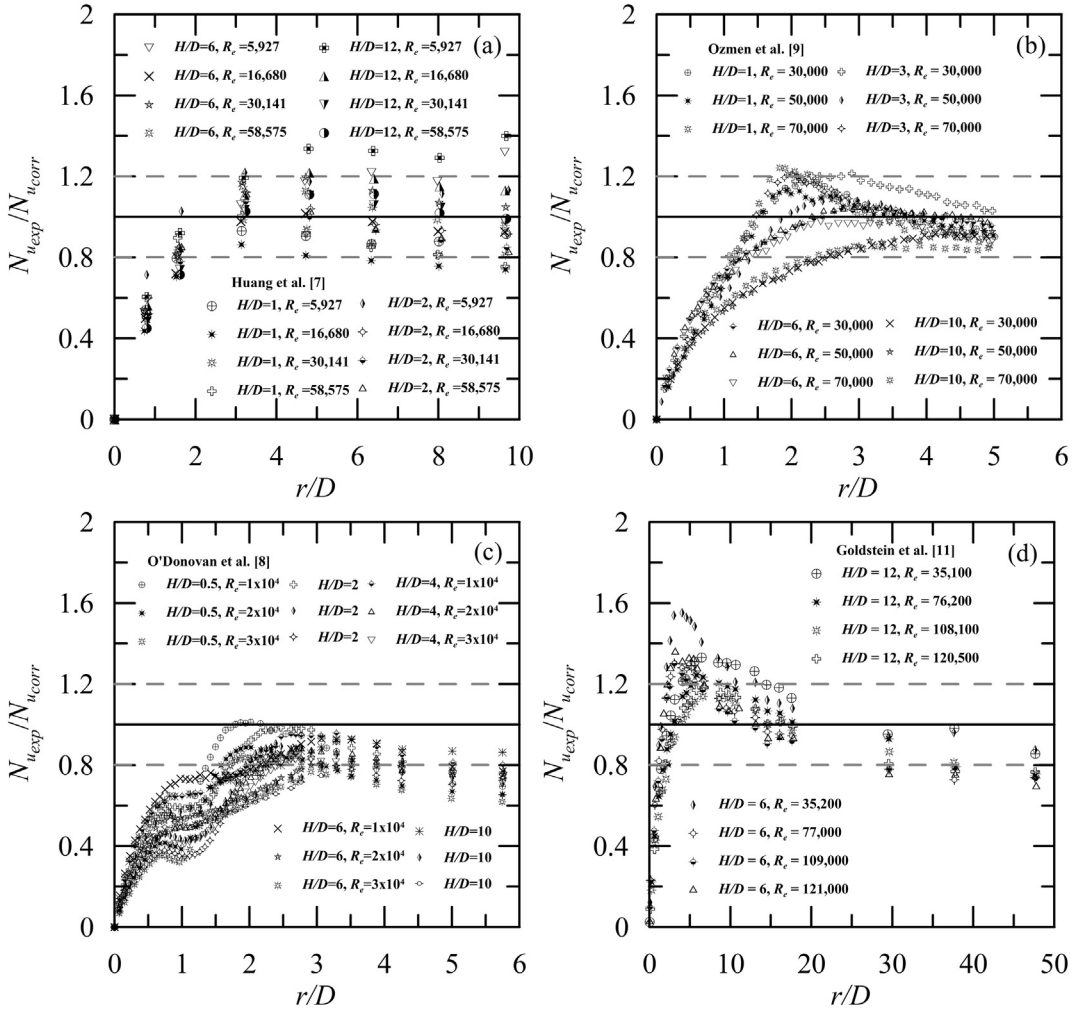

Fig. 12. Comparison of the modified Gardon and Cobonpue correlation [32] with the experimental data of: (a) Huang and El-Genk [7], (b) Ozmen and Baydar [9], (c) O'Donovan and Murray [8] and (d) Goldstein and Behbahani [11].

approximation. The critical parameter for an improvement in the performance of the correlations is not H/D, but rather the exponent of the Reynolds number.

Equations shown in Table 5 are generalizations of the formulations discussed previously. The value of each constant was obtained through a non-linear regression applied simultaneously to the data of [7–9,11]. The first equation shown in Table 5 is based on the correlation of Liu et al. [20], whose fitting to the experimental data provides a coefficient of determination of 0.964. If the power of the Reynolds number is allowed to vary, 0.5 changes to 0.656 with R-sq = 0.973. The dependence on H/D is considered next and is shown to be very mild ($c = -0.009$). The last equation in Table 5 is referred to the correlation of Katti and Prabhu [10].

The above discussion suggests the present work to use the correlation suggested by Ozmen and Baydar [9], but with the new values (Table 5) shown below

$$N_{u_0} = 0.159 R_e^{0.66} P_r^{1/3}. \tag{11}$$

Eq. (11) is valid for the prediction of the stagnation Nusselt number in confined and unconfined jets, in the ranges $0.5 < H/D < 12$ and $6,000 < R_e < 121,000$.

The adequacy of Eq. (11) is graphically verified through Fig. 11a and 11b. For the range of jet configurations investigated, Eq. (11) represents all experimental data to within ± 20% accuracy. The highest dispersion is observed for $H/D = 6$, where peak values of N_{u_0} are expected to happen.

5.3. Nusselt number correlations: radial distribution

The correlations for Nusselt number listed in Table 2 are tested against the experimental data of [7–9,11]. For this set, the experimental conditions include confined and unconfined jets with a Reynols number variation from 6,000 to 121,000; the nozzle-to-plate spacing (H/D) ranges from 0.5 to 12.

The results show that the parametric relation of Liu et al. [20] considerably underestimates the experimental values.

A serious difficulty with the equation proposed by Martin [35] is the limiting bevahior as $r/D \to 0$ since Nusselt number falls dramatically to negative values before blowing out to infinity. In view of the described non-physical behavior, this equation is not further considered.

The work of Katti and Prabhu [10] is unique in proposing three different correlations, valid in specific regions of the domain (see Fig. 4 and Table 2).

A non-linear fitting procedure was applied to the correlations of Gardon and Cobonpue [32], Huang and El-Genk [7], Goldstein et al. [33], Jambunathan et al. [34] and Katti and Prabhu [10], to determine new constants, as implied by the data of references [7–9,11]. Figs. 12–16 show the agreement of every modified corre-

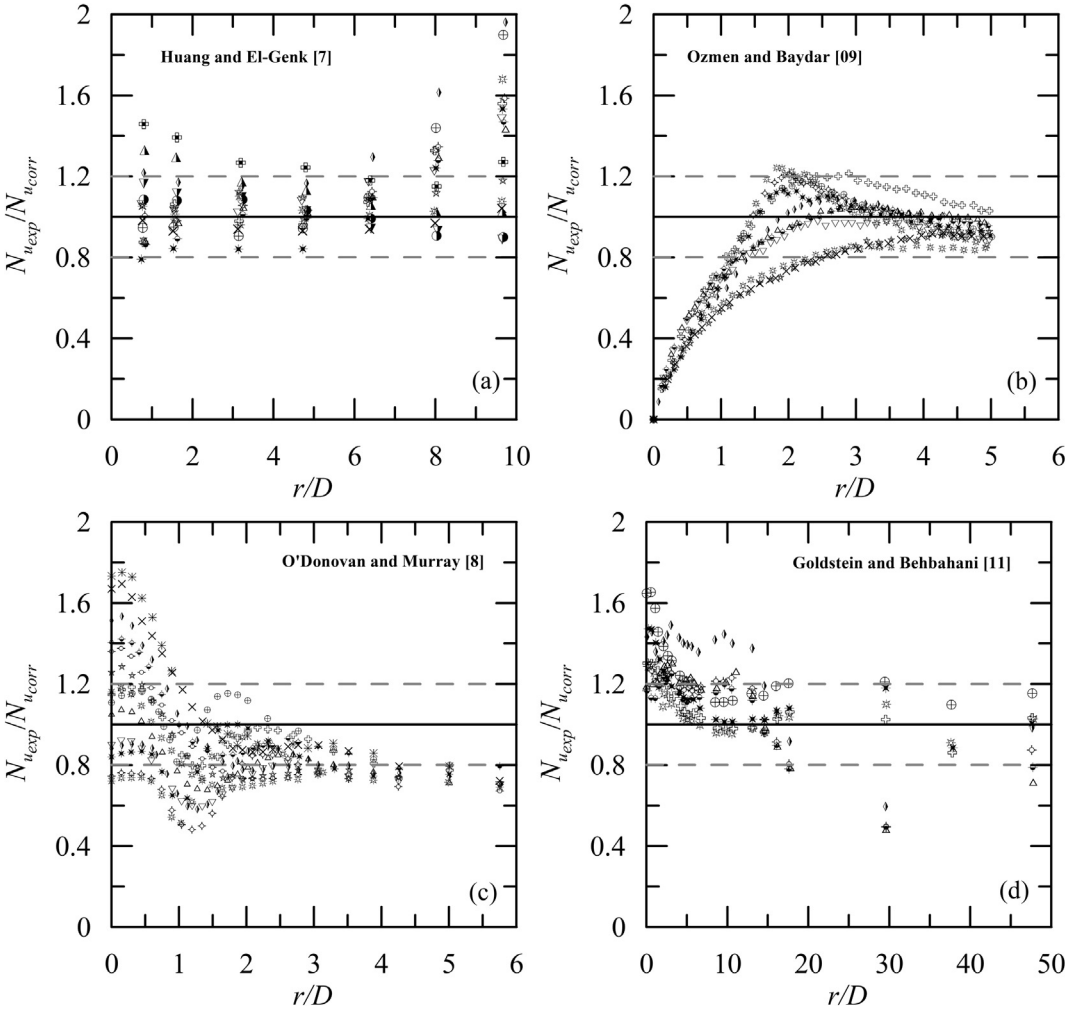

Fig. 13. Comparison of the modified Huang and El-Genk [7] correlation with the experimental data of: (a) Huang and El-Genk [7], (b) Ozmen and Baydar [9], (c) O'Donovan and Murray [8] and (d) Goldstein and Behbahani [11]. Symbols are the same as in Fig. 12.

lation in comparison to every group of experimental result. Note that the complete data set is considered in the implementation of the non-linear fitting procedure. However, the modified equations are compared with the results of every experimental work for the purpose of clarification.

Fig. 12a–d show estimations of Nusselt number for the modified Gardon and Cobonpue correlation [32] in comparison to the data of Huang and El-Genk [7], Ozmen and Baydar [9], O'Donovan and Murray [8] and Goldstein and Behbahani [11]. Predictions in the region $r/D < 2.5$ show a large discrepancy with the experimental results. In fact, the predictions as compared to the results of references [7,9] shown agreement to within ± 20%; a comparison against the data of references [8,11] results very poor. The adjusted fitting furnishes a R-squared value of 0.982.

Results for the modified Huang and El-Genk [7] correlation are shown in Fig. 13a-d. This parametrization is based on three constants (a, b and c, see Table 2), that are described as fourth order polynomial functions of r/D. The fitting procedure adjusted fifteen constants to the experimental data, resulting in a R-squared value of 0.985. The agreement with the data of references [9,11] is good (Fig. 13b, d), but larger discrepancies are found for the interval $r/D > 7$ of the data of reference [7] (Fig. 13a).

The predictive capability of the modified Goldstein et al. [33] equation is tested in Fig. 14a-d. Deviations larger than ± 20% are observed for the data of Huang and El-Genk [7] (Fig. 14a) and [11] (Fig. 14d). The fitting statistics give a R-squared value of 0.985.

Fig. 15a presents good agreement between the modified Jambunathan correlation [34] and the data of Huang and El-Genk [7], except for the condition $H/D = 12$, $R_e = 5,927$ (Fig. 15a). Fig. 15d shows that the modified Jambunathan correlation is not appropriate to represent Nusselt number behavior for large values of r/D. The predictions given by the correlations of references [8,9] are only reasonable (Fig. 15b,c).

In respect to the correlation based on the work of Katti and Prabhu [10], three fitting procedures were carried out to adjust the expressions to the stagnation, transition and wall jet regions. The results are shown in Fig. 16a-d. Poor agreement is observed for the data of Huang and El-Genk [7] (Fig. 16a) for the lowest Reynolds number and $H/D = 6$ and 12. Similar results are observed for the data of Goldstein and Behbahani [11] (Fig. 16d) and the same lower R_e and H/D conditions. A good agreement is observed for the experimental data of Ozmen and Baydar and O'Donovan and Murray [8,9] (Fig. 16b,c). The discrepancies observed in Fig. 16c are due to the peak values of N_u observed for $H/D < 4$. In fact, none of the correlations investigated in the present work were capable of predicting the magnitude and position of peak values in the Nusselt distribution.

Figs. 12–16 show that the correlation that provides the better agreement and the smallest discrepancy between the parametric

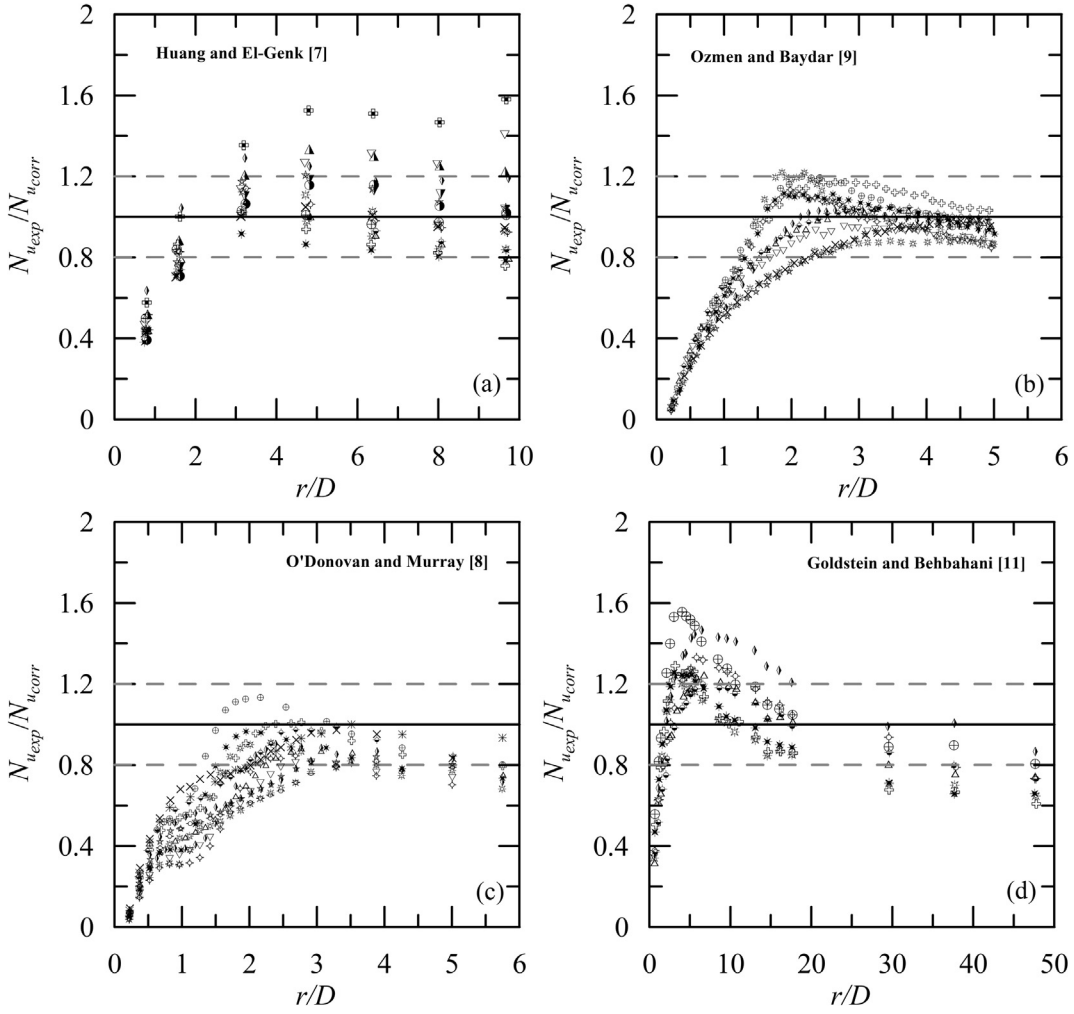

Fig. 14. Comparison of the modified Goldstein et al. [33] correlation with the experimental data of: (a) Huang and El-Genk [7], (b) Ozmen and Baydar [9], (c) O'Donovan and Murray [8] and (d) Goldstein and Behbahani [11]. Symbols are the same as in Fig. 12.

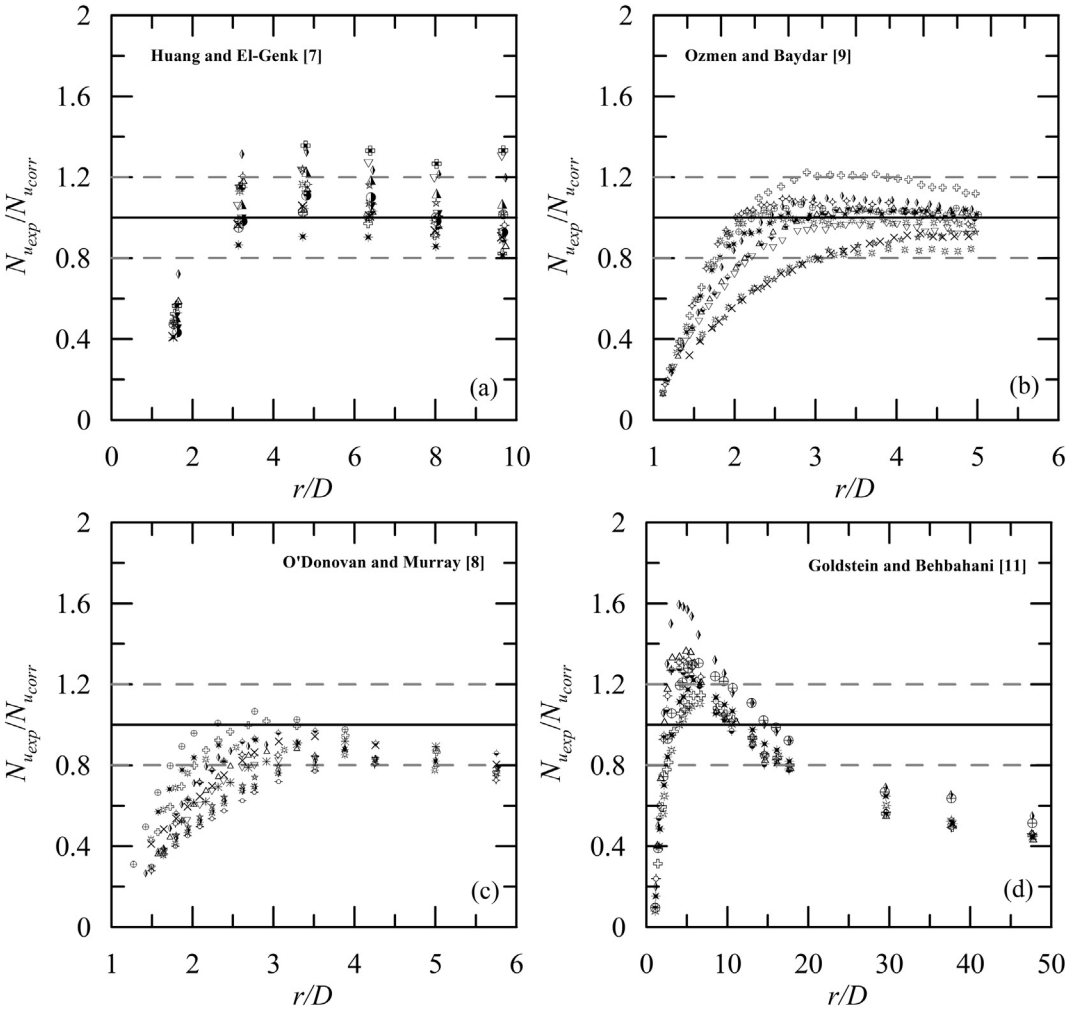

Fig. 15. Comparison of the modified Jambunathan et al. [34] correlation with the experimental data of: (a) Huang and El-Genk [7], (b) Ozmen and Baydar [9], (c) O'Donovan and Murray [8] and (d) Goldstein and Behbahani [11]. Symbols are the same as in Fig. 12.

prediction and the experimental results is the modified Katti and Prabhu [10] equation.

5.4. Nusselt number in the stagnation region ($0 < r/D < 1$)

According to the modified Katti and Prabhu [10] equation, the stagnation region is modeled through

$$N_u = a(H/D)^b R_e^{0.66} P_r^{1/3} \left(1 - \frac{(r/D)^2 (H/D)^{-0.2}}{c}\right)^{1.2}, \quad (12)$$

where the Reynolds number exponent 0.66 is fixed to keep coherence with Eq. (11). The fitting procedure gives a R-squared coefficient of determination of 0.976. The full statistical properties are presented in Table 6.

5.5. Nusselt number in the transition region ($1 < r/D < 2.5$)

The transition region of the impinging jet configuration, $1 < r/D < 2.5$, is also modeled according to the modified Katti and Prabhu [10] equation as

$$N_u = a(H/D)^b (r/D)^c R_e^{0.8} P_r^{1/3}, \quad (13)$$

where the exponent of the Reynolds number was adjusted to 0.8 to match the exponent used in the wall jet region. This value also maximizes the fitting coefficient of determination (=0.973). The fitting statistical properties are presented in Table 7.

5.6. Nusselt number in the wall jet region ($r/D > 2.5$)

In the wall jet region, the boundary layer is fully turbulent. Thus, integral solutions for the boundary layer suggest N_u to scale with R_e and P_r according to

$$N_u = a(H/D)^b (r/D)^c R_e^{0.8} P_r^{1/3}. \quad (14)$$

The wall jet region is the region that covers most of the affected flow area. The functional form of Eq. (14) is the same of that of Eq. (13). The constants of the distinct flow regions, however, are different.

An estimation of the parameters a, b and c for the region $r/D > 2.5$ on the basis of the data of references [7–9,11] gives the results presented in Table 8 (R-sq = 0.984).

5.7. Overall Nusselt number

The combination of all four predictive equations for N_u (Eqs. (11)–(14)) gives results that are valid for confined and unconfined jets, for the range of conditions given by $6,000 < R_e < 121,000$, $0.5 < H/D < 12$, $0 < r/D < 50$.

The predictive equations are compared with the experimental data of Fenot et al. [37] in Fig. 17a,b,c for jets with $H/D = 5$ (confined and unconfined) and $H/D = 2$ (confined). The data of Fenot

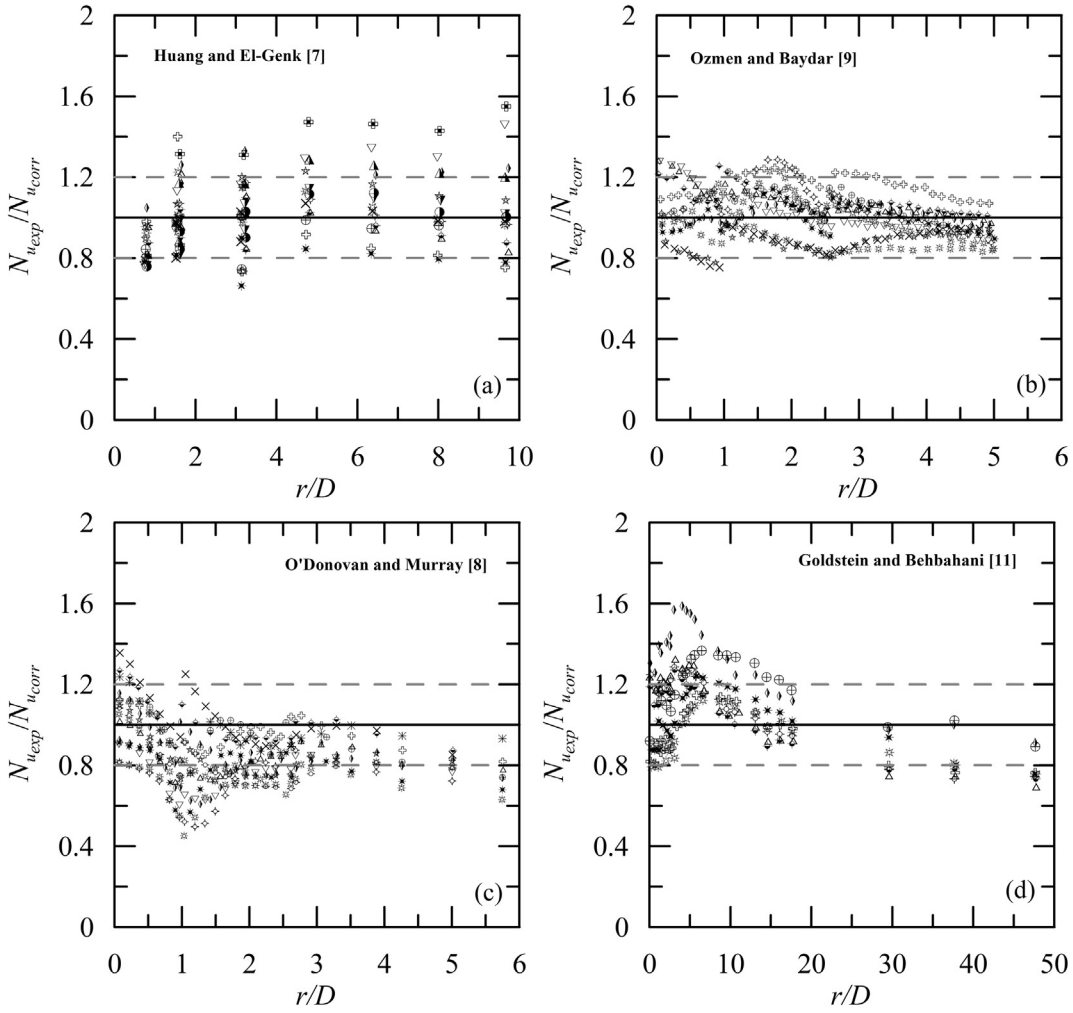

Fig. 16. Evaluation of the modified Katti and Prabhu [10] correlation against the data of: (a) Huang and El-Genk [7], (b) Ozmen and Baydar [9], (c) O'Donovan and Murray [8] and (d) Goldstein and Behbahani [11]. Symbols are the same as in Fig. 12.

Table 6
Fitting statistics to the stagnation region, Eq. (12).

Constant	Estimate	Standard error	Confidence interval	Confidence level (%)
a	0.155	0.002	0.149, 0.159	95
b	−0.023	0.009	−0.040, −0.006	95
c	8.246	0.938	6.402, 10.091	95

Table 7
Fitting statistics to the transition region, Eq. (13).

Constant	Estimate	Standard error	Confidence interval	Confidence level (%)
a	0.035	0.001	0.034, 0.036	95
b	−0.153	0.006	−0.167, −0.140	95
c	−0.227	0.021	−0.268, −0.187	95

Table 8
Fitting statistics to the wall jet correlation, Eq. (14).

Constant	Estimate	Standard error	Confidence interval	Confidence level (%)
a	0.050	0.001	0.048, 0.051	95
b	−0.071	0.005	−0.081, −0.061	95
c	−0.804	0.014	−0.830, −0.776	95

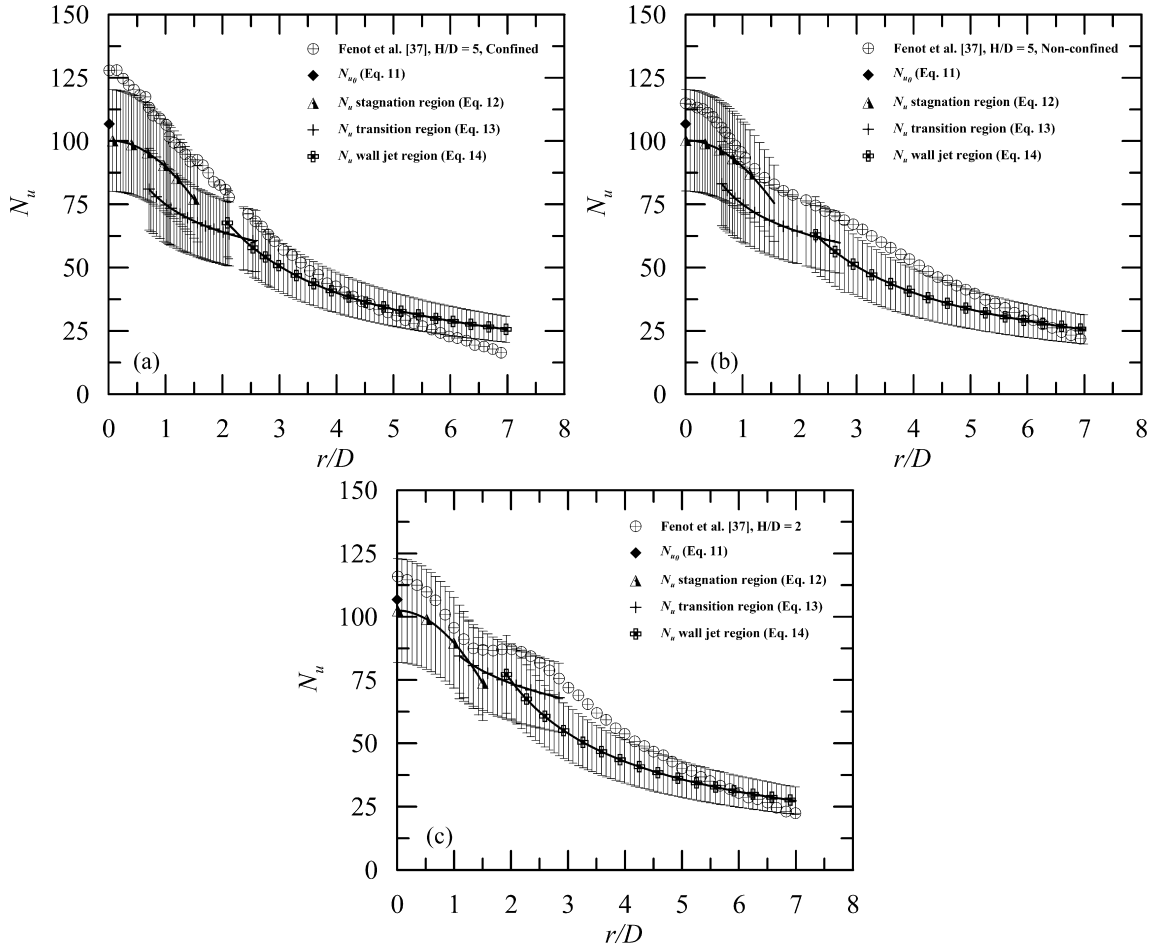

Fig. 17. Global predicted behavior of N_u.

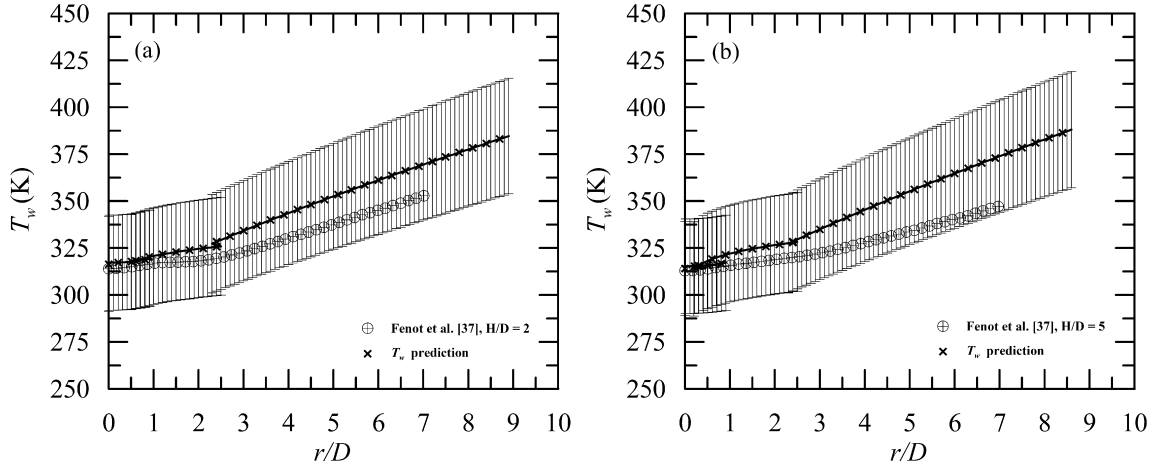

Fig. 18. Global behavior of the wall temperature T_w.

et al. [37] were not used in the fitting procedures that resulted in the predictive equations for the Nusselt number. The data are used here for an independent assessment of the proposed correlations.

The error bars shown in Fig. 17a-c express an uncertainty of ± 20%. As can be seen, the predictions for all three different investigated configurations show a good agreement with the experimental data.

In situations where the wall heat flux (q_w) is a known quantity, the predictive N_u equations, Eqs. (11)–(14), can be used to evaluate the wall temperature T_w. Fig. 18a and b show a comparison between the predicted wall temperature and the experimental measurement of Fenot et al. [37] for $H/D = 2$ and 5, respectively. The agreement is very good, within ±8% of the reference data, as expressed by the error bars.

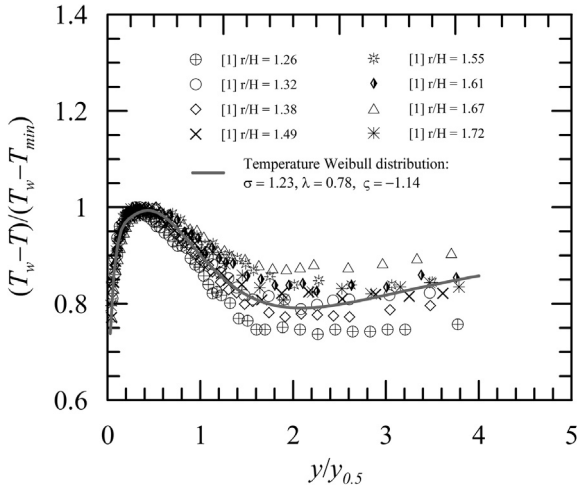

Fig. 19. Weibull distribution for the radial mean temperature profiles of Guerra et al. [1].

Table 9
Summary of proposed parameters.

Equation	Parameter	Reference
(1)	$\gamma = 1.32$, $\beta = 0.73$	[2]
(3)	$A_1 = 0.962$, $A_2 = 9$	[2]
(6)	$m_1 = -1, C_1 = 2.72$	Present
(7)	$m_2 = 1$, $C_2 = 0.0175$	Present
(11)	a = 0.159, b =0.66	Present
(12)	a = 0.155, b = −0.023, c = 8.246	Present
(13)	a = 0.035, b = −0.153, c = −0.23	Present
(14)	a = 0.05, b = −0.07, c = −0.80	Present
(8)	$B_1 = 1.003$, $B_2 = 9.462$	[1]
(10)	$\sigma = 1.23$, $\lambda = 0.78$, $\zeta = -1.14$	Present

5.8. Temperature profile in the wall jet region

Temperature profiles are seldom presented in experimental or numerical works. However, they are important to characterize T_{min} and test Eq. (10). To validate Eq. (10) we used the only set of experimental data that could be found in literature, the data of Guerra et al. [1]. The agreement with the proposed Weibull distribution, Eq. (10), is shown in Fig. 19 with $\sigma = 1.23$, $\lambda = 0.78$ and $\zeta = -1.14$.

6. Final remarks

In the course of the present study, 123 articles were examined for data extraction. In the end, only eleven contained all the necessary information for the validation of Eqs. (1)–(14). These data cover a large range of conditions, thus rendering great generality to the present approach.

A deficient aspect of the available literature data is the almost non-existent information on temperature profiles. Studies on the behavior of the mean and fluctuating temperatures must be pursued in the future.

The present work offers a complete picture of the jet impingement phenomenon and can be used to provide simple formulations to many problems of engineering interest, in particular, concerning parameters whose description in literature are difficult to find. The radial distributions of wall shear stress and temperature (at the wall and away from it) characterize some of these cases.

A summary of the proposed correlations is presented in Table 9.

Acknowledgements

In the course of the research, JBRL benefited from a CNPq Research Fellowship (Grant No 308445/2013-9) and from further financial support through Grants CNPq 458249/2014-9, FAPERJ E-26/102.212/2013 and FAPERJ E-26/010.002857/2014. APSF is grateful to the Brazilian National Research Council (CNPq) for the award of a Research Fellowship (Grant No 305338/2014-5). The work was financially supported by the Rio de Janeiro Research Foundation (FAPERJ) through Grant E-26/202.912/2015.

References

[1] D.R.S. Guerra, J. Su, A.P. Silva Freire, The near wall behaviour of an impinging jet, Int. J. Heat Mass Transfer 48 (2005) 2829–2840.
[2] J.B.R. Loureiro, A.P. Silva Freire, Wall shear stress measurements and parametric analysis of impinging wall jets, Int. J. Heat Mass Transfer 55 (2012) 6400–6409.
[3] M. Poreh, Y.G. Tsuei, J.E. Cermak, Investigation of a turbulent radial wall jet, Trans. ASME: J. Appl. Mech. 34 (1967) 457–463.
[4] M. Fairweather, G.K. Hargrave, Experimental investigation of an axisymmetric, impinging turbulent jet. Part 1: velocity field, Exp. Fluids 33 (2002) 464–471.
[5] J.A. Fitzgerald, S.V. Garimella, A study of the flow field of a confined and submerged impinging jet, Int. J. Heat Mass Transfer 41 (1998) 1025–1034.
[6] M.F. Koseoglu, S. Baskayab, The effect of flow field and turbulence on heat transfer characteristics of confined circular and elliptic impinging jets, Int. J. Therm. Sci. 47 (2008) 1332–1346.
[7] L. Huang, M.S. El-Genk, Heat transfer of an impinging jet on a flat surface, Int. J. Heat Mass Transfer 37 (1994) 1915–1923.
[8] T.S. O' Donovan, D.B. Murray, Jet impingement heat transfer – Part I: mean and root-mean-square heat transfer and velocity distributions, Int. J. Heat Mass Transfer 50 (2007) 3291–3301.
[9] Y. Ozmen, E. Baydar, Flow structure and heat transfer characteristics of an unconfined impinging air jet at high jet Reynolds numbers, Heat Mass Transfer 44 (2008) 1315–1322.
[10] V. Katti, S.V. Prabhu, Experimental study and theoretical analysis of local heat transfer distribution between smooth flat surface and impinging air jet from a circular straight pipe nozzle, Int. J. Heat Mass Transfer 51 (2008) 4480–4495.
[11] R.J. Goldstein, A.I. Behbahani, Impingement of a circular jet with and without cross flow, Int. J. Heat Mass Transfer 25 (1982) 1377–1382.
[12] K.R. Sreenivasan, A unified view of the origin and morphology of the turbulent boundary layer structure, in: H.W. Liepmann, R. Narasimha (Eds.), Turbulence Management and Relaminarization, 1987.
[13] R. Narasimha, K.Y. Narayan, S.P. Pathasarathy, Parametric analysis of turbulent wall jets in still air, Aeronaut. J. 77 (1973) 335–339.
[14] N. Uddin, S.O. Neumann, B. Weigand, LES simulations of an impinging jet: on the origin of the second peak in the Nusselt number distribution, Int. J. Heat Mass Transfer 57 (2013) 356–368.
[15] E. Pulat, M.K. Isman, A.B. Etemoglu, M. Can, Effect of turbulence models and near-wall modeling approaches on numerical results in impingement heat transfer, Numer. Heat Transfer, Part B 60 (2011) 486–519.
[16] I.B. Özdemir, J.H. Whitelaw, Impingement of an axisymmetric jet on unheated and heated flat plates, J. Fluid Mech. 24 (1992) 503–532.
[17] C.O. Popiel, O. Trass, Visualization of a free and impinging round jet, Exp. Therm. Fluid Sci. 4 (1991) 253–264.
[18] M. Hadziabdi, K. Hanjalic, Vortical structures and heat transfer in a round impinging jet, J. Fluid Mech. 596 (2008) 221–260.
[19] D.J. Phares, G.T. Smedley, R. Flagan, The wall shear stress produced by the normal impingement of a jet on a flat surface, J. Fluid Mech. 418 (2000) 351–375.
[20] X. Liu, J.H. Lienhard V, J.S. Lombara, Convective heat transfer by impingement of circular liquid jets, J. Heat Transfer 113 (1991) 571–582.
[21] C.D. Donaldson, R.S. Snedeker, P.D. Margolis, A study of free jet turbulent structure and impingement heat transfer, J. Fluid Mech. 45 (1971) 477–512.
[22] D. Lytle, B.W. Webb, Secondary heat transfer maxima for air jet impingement at low nozzle-to-plate spacing, Exp. Heat Transfer Fluid Mech. Thermodyn. (1991) 776–783.
[23] J.Y. San, W.Z. Shiao, Effects of jet plate size and plate spacing on the stagnation Nusselt number for a confined circular air jet impinging on a flat surface, Int. J. Heat Mass Transfer 49 (2006) 3477–3486.
[24] T. Liu, J.P. Sullivan, Heat transfer and flow structures in an excited circular impinging jet, Int. J. Heat Mass Transfer 39 (1996) 3695–3706.
[25] S.V. Garimella, R.A. Rice, Confined and submerged liquid jet impingement heat transfer, J. Heat Transfer – Trans. ASME 117 (1995) 871–877.
[26] D.A. Zumbrunnen, M. Aziz, Convective heat-transfer enhancement due to intermittency in an impinging jet, J. Heat Transfer – Trans. ASME 115 (1993) 91–98.
[27] A.K. Mohanty, A.A. Tawfek, Heat transfer due to a round jet impinging normal to a flat surface, Int. J. Heat Mass Transfer 36 (1993) 1639–1647.
[28] P.M. Brdlik, V.K. Savin, Heat transfer in the vicinity of stagnation point in an axisymmetric jet flowing flat surfaces normal to the flow, J. Eng. Phys. 10 (1966) 423–428.
[29] T. Persoons, A. McGuinn, D.B. Murray, A general correlation for the stagnation point Nusselt number of an axisymmetric impinging synthetic jet, Int. J. Heat Mass Transfer 54 (2011) 3900–3908.

[30] R. Viskanta, Heat transfer to impinging isothermal gas and flames, Exp. Therm. Fluid Sci. 6 (1993) 111–134.
[31] P.S. Shadelsky, Stagnation point heat transfer for jet impingement to a plane surface, AIAA J. 21 (1983) 1214–1215.
[32] R. Gardon, J. Cobonpue, Heat transfer between a flat plate and jets of air impinging on it, Int. Dev. Heat Transfer, A.S.M.E., New York (1962) 454–460.
[33] R.J. Goldstein, A.I. Behbahani, K. Kieger Heppelmann, Streamwise distribution of the recovery factor and the local heat transfer coefficient to an impinging circular air jet, Int. J. Heat Mass Transfer 29 (1986) 1227–1235.
[34] K. Jambunathan, E. Lai, M.A. Moss, B.L. Button, A review of heat transfer data for single circular jet impingement, Int. J. Heat Fluid Flow 13 (1992) 106–115.
[35] H. Martin, Heat and mass transfer between impinging gas jets and solid surfaces, Adv. Heat Transfer 13 (1997) 1–60.
[36] J.B.R. Loureiro, F.B.C.C. Sousa, J.L.Z. Zotin, A.P. Silva Freire, The distribution of wall shear stress downstream of a change in roughness, Int. J. Heat Fluid Flow 31 (2010) 785–793.
[37] M. Fenot, J.J. Vullierme, E. Dorignac, Local heat transfer due to several configurations of circular air jets impinging on a flat plate with and without semi-confinement, Int. J. Therm. Sci. 44 (2005) 665–675.